Summary report for special agreement TAL-NAPC20220804-002

Cédric JOUANNE

December 8, 2022

1   Introduction

This document presents a comparative analysis of neutron-Fe56 (iron is almost 92% Fe56) interaction evaluation files, in particular for elastic and inelastic scattering. First, the cross sections as a function of incident energy will be compared. Secondly, the scattering anisotropies will be studied, as they drive the neutron energy transfer and thus play a very important role in neutron propagation. Shielding and criticality configurations will be studied as well as slowing down simulations in a mono-atomic medium.

2   Nuclear data analysis

Figure 1 presents the pointwise Fe56 elastic cross section at 294 K from five libraries:

- ENDF/B-VIII [1] (RRR $[10^{-5}\,eV \to 850\,keV]$, Reich-Moore formalism) in black

- JEFF-3.3 [2] (RRR $[10^{-5}\,eV \to 850\,keV]$, Reich-Moore formalism) in red

- JEFF-4.0T1 [3] (RRR $[10^{-5}\,eV \to 2\,MeV]$, R-Matrix Limited) in green

- JENDL-5 [4] (RRR $[10^{-5}\,eV \to 850\,keV]$, Reich-Moore formalism) in blue

- TENDL21 [5, 6] (RRR $[10^{-5}\,eV \to 850\,keV]$, Reich-Moore formalism) in orange

All these cross-sections have about 40,000 points and so comparison is visually difficult. Figure 2 shows a groupwise representation of the elastic cross-section using a 100 keV bining. We can observe a disparity in the cross sections in the resolved range that ends around 2 MeV and around 3 MeV.

We are interested in compositions containing iron with neutron sources that have energy components above 2 or 3 MeV. The first three excited states of Fe56 are at energies of 0.847, 2.085 and 2.658 MeV respectively. Scattering is the most probable collision, accounting for
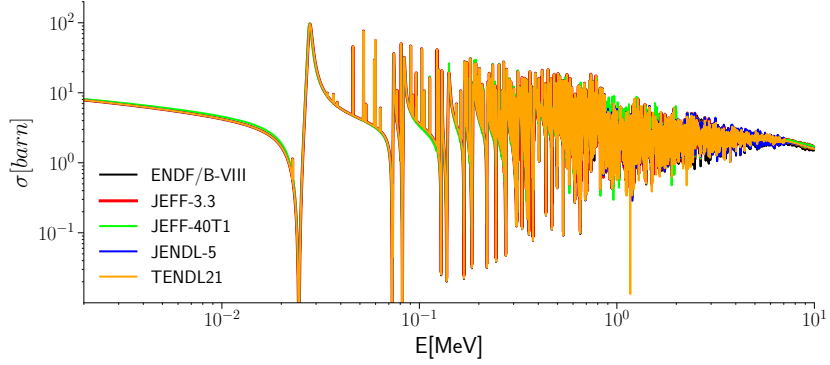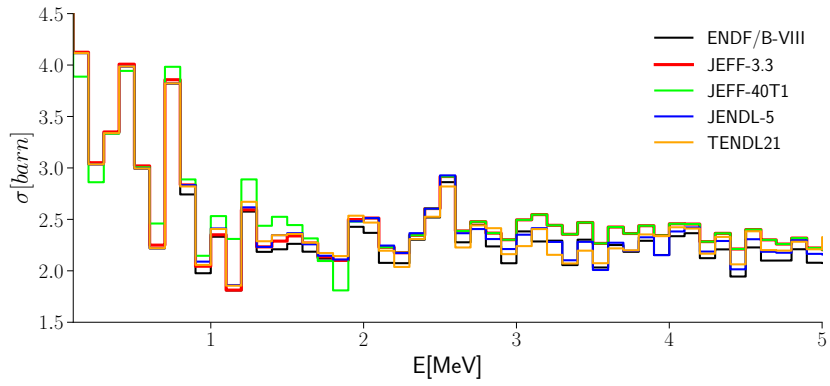
Figure 1: Fe56 pointwise elastic cross-sections

Figure 2: Fe56 groupwise elastic cross-sections

nearly 100% of the interactions between 1 and 5 MeV, it is important to focus on inelastic scattering which plays a very important role in neutron kinematics. In an elastic collision, the energy lost by the neutron in the laboratory frame is directly connected to the scattering angle in the centre of mass frame. If we consider E, the initial energy of the neutron in the laboratory frame, θ the angle of the elastic scattering in the centre of mass frame and A the mass of the target in terms of neutron mass, the energy of the neutron E' in the laboratory frame after the collision is given by the relation :

$$E' = E\frac{1}{2}\big[1 + \alpha + (1 - \alpha)\cos\theta\big]$$

where :

$$\alpha = \left(\frac{A-1}{A+1}\right)^2$$

For elastic scattering on an Fe56, the neutron can therefore lose up to 7% of its kinetic energy During an inelastic collision, the neutron will lose at least the energy corresponding to the

excited level reached by the collided nucleus, i.e. approximately 850 keV, 2.1 MeV and 2.7 MeV for the first three excited states. Figure 3 and Figure 4 present respectively the cross-sections and the ratio to the elastic scattering cross for the inelastic scattering to the first excited state (MT51, 850 keV). We observe a significant difference between ENDF/B-VIII and
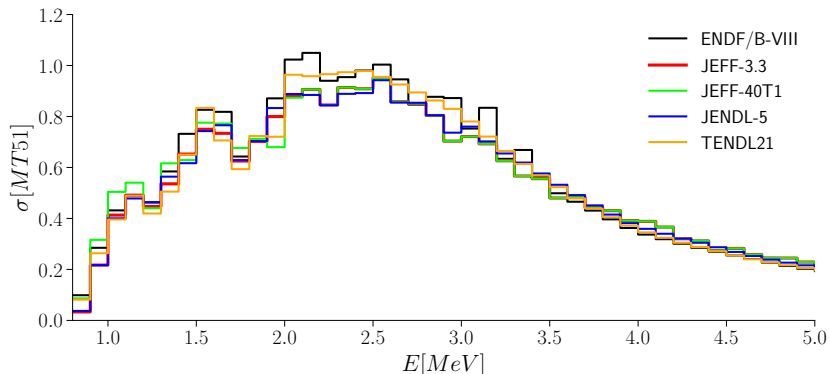

Figure 3: Fe56 groupwise cross-sections for inelastic scattering to the first excited state (MT51)
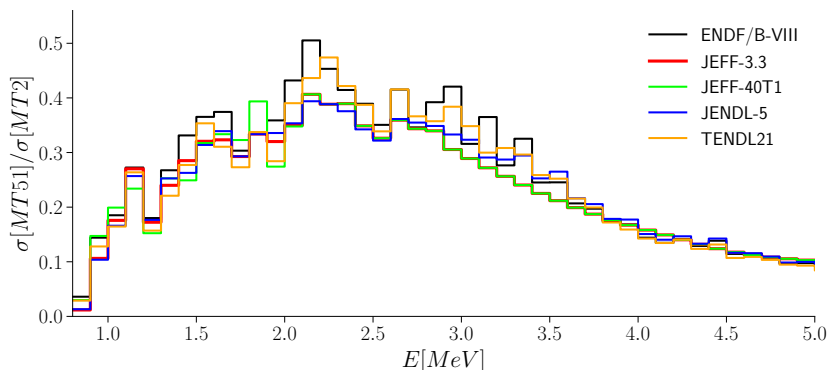

Figure 4: Fe56 groupwise ratio $\sigma(MT51)/\sigma(MT2)$

JEFF-3/JEFF-40-T1 for energies of 2 and 3 MeV. We will later study the slowing down of a 3 MeV neutron source to investigate this energy range.

Above 3 MeV, the cross-section of the MT51 reaction decreases, the inelastic scattering towards the higher excited states becomes more important. Figure 5 and Figure 6 show the total inelastic scattering cross sections (MT4) and the ratio to the elastic scattering cross section (MT2). The higher the excited state, the more energy the neutron will lose in the reaction. Above 4 MeV, inelastic scattering contributes about 1/3 of the total cross section. This indicates the importance of the MT4/MT2 ratio for neutron kinematics around these energies. The lower the ratio, the more neutrons will propagate in the steel.
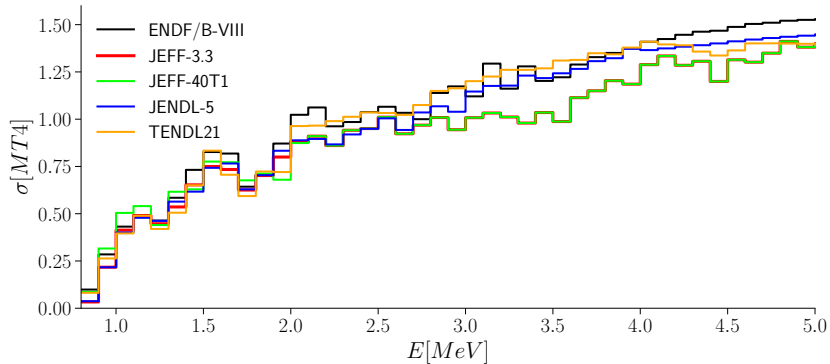
Figure 5: Fe56 groupwise cross-sections for total inelastic scattering (MT4)
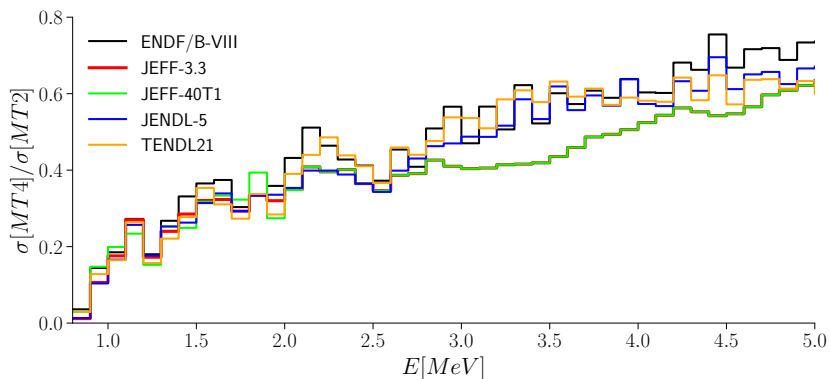

Figure 6: Fe56 groupwise ratio $\sigma(MT4)/\sigma(MT2)$

2.1 Scattering anisotropy

For configurations that contain iron and for neutron energies of a few hundred kev to a few MeV, the anisotropy of the reactions is very important. This is particularly the case for elastic scattering, due to the bijection between the cosine of the scattering angle in the centre-of-mass reference frame and the energy of the neutron dissociated from this scattering. Figure 7 shows the average cosines on a multi-group mesh of the elastic scattering. The closer the cosine is to 1, the less energy the neutron loses during the collision. The maximum transfer, for a cosine equal to -1, is 7 percent for Fe56.

The resonance parameters in the resolved domain of Fe56 are given with the R-Matrix-Limited formalism for the JEFF-40T1 evaluation. It is therefore possible to compare the anisotropy given in the MF=4 evaluation with that calculated using the resonance parameters in the resolved domain which ends at 2 MeV for this evaluation. We observe large deviations in the average anisotropy over this energy range, which will result in significant effects on neutron transport in Fe56 material.

4

We also observe that above 2.5 MeV, the mean cosine in the TENDL21 evaluation has a linear upward trend compared to the other evaluations.

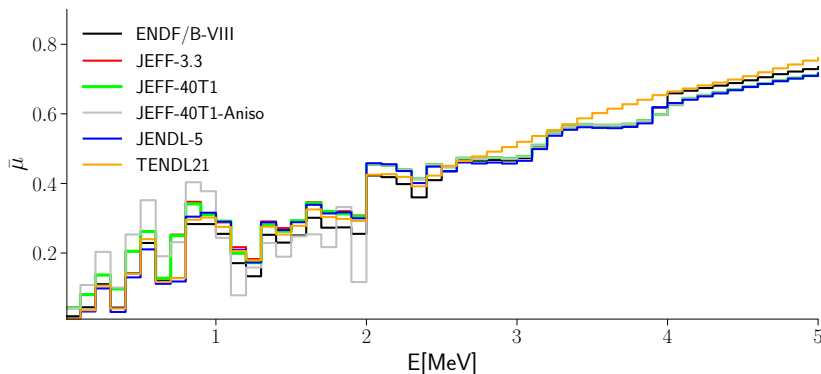
Figure 7: Fe56 groupwise average cosine for elastic scattering

3   Slowing down in an iron sphere

The configurations considered in this section are 30cm radius spheres composed solely of Fe56 with a density of 7.8 g/cm^3. Two sources are simulated: 850 keV and 3 MeV, a bining of 20 keV is used to compare the neutron flux in the sphere. Calculations were made with MCNP6.1 and TRIPOLI-4. Figure 8 shows flux for the two sources (850 keV and 3 MeV).
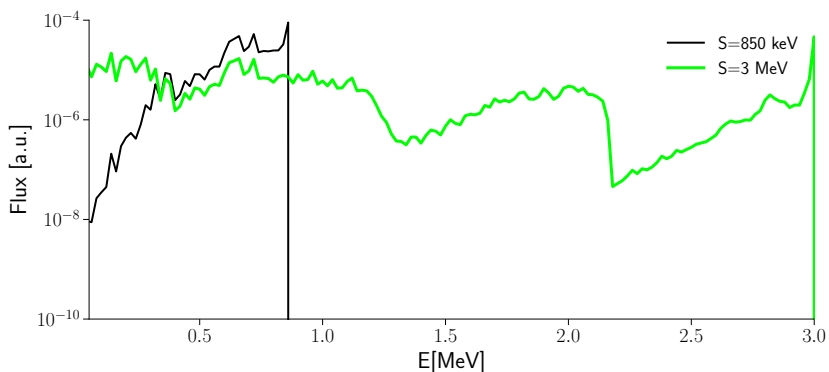

Figure 8: Fe56 groupwise average cosine for elastic scattering

The following figures show the relative deviations to a calculation performed with MCNP6.1 and the ENDF/B-VIII library. In addition to the T4 calculations performed with the previous libraries, a JEFF-4.0T1 Fe56 file and the anisotropy reconstructed using the resonance parameters, noted JEFF-40T1+aniso, is presented.

5

Figure 9 shows the results for a monokinetic neutron source at 850 keV for which only elastic scattering and radiative capture exist. The difference between the JEFF-40T1 calculations without and with the anisotropy reconstructed by the resonance parameters is very large.
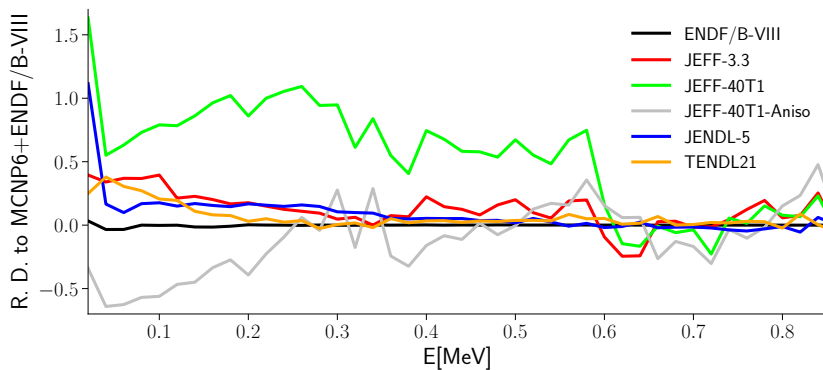

Figure 9: Fe56 Slowing down 850 keV

Figure 10 shows the results for a monokinetic neutron source at 3 MeV. At this energy, inelastic scattering to the first four excited states is possible. The breakdown of trends around 2.2 MeV and 1.3 MeV indicate the importance of inelastic scattering to the first excited state in these calculations.
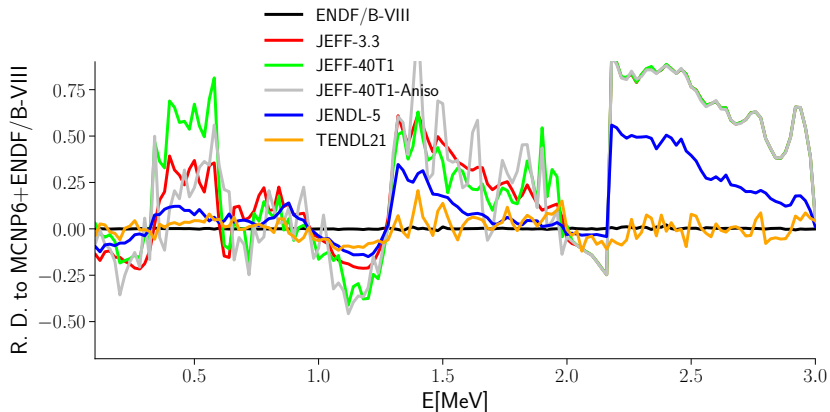

Figure 10: Fe56 Slowing down 3 MeV

In order to estimate the impact of the elastic scattering anisotropy, calculations were made with the cross sections of the elastic scattering from the different evaluations and the elastic anisotropy data from ENDF/B-VIII. These calculations with T4 are shown in Figure 11 and are

therefore to be compared with those in Figure 9. We note that the differences in anisotropies explain the differences between ENDF/B-VIII, JENDL-5 and TENDL-21. For JEFF-3.3 and JEFF-40T1, this does not explain the differences, especially for JEFF-40T1 with a large deviation more likely related to the cross-section $\sigma_{el.}(E)$.
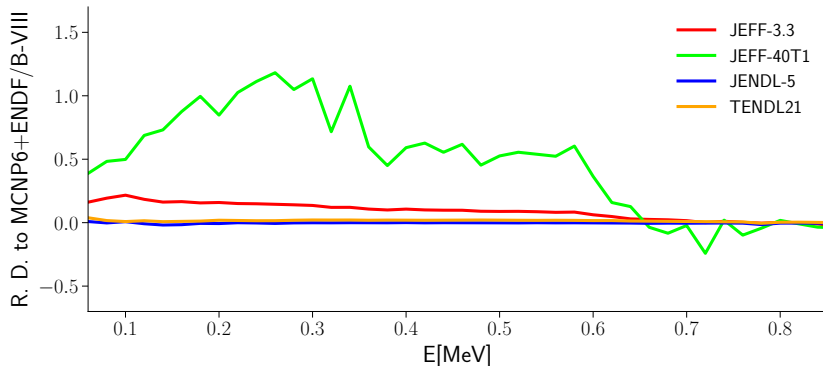

Figure 11: Fe56 Slowing down 850 keV aniso B8

In order to quantify the impact of the differences in the inelastic scattering cross sections between the ENDF/B-VIII and JEFF-3.3 evaluations, the inelastic scattering cross sections from the JEFF-3.3 evaluation were progressively replaced by those from ENDF/B-VIII. Figure 12 shows the respective relative deviations from a MCNP+ENDF/B-VIII calculation with a 3 MeV source for the following calculations:

- T4 + ENDF/B-VIII in black

- T4 + JEFF-33 in red

- T4 + JEFF-33 with MF3/MT51 of ENDF/B-VIII in green

- T4 + JEFF-33 with MF3/MT51-52 of ENDF/B-VIII in orange

- T4 + JEFF-33 with MF3/MT51-52-53 of ENDF/B-VIII in blue

The attenuation of the discrepancies is very important in the energy range from 1.3 MeV to 3 MeV. The competition between elastic and inelastic scattering is therefore the important point for neutrons with energies above 1 MeV for this Fe56 nucleus. The analysis of the results on the ASPIS benchmark in the next section will confirm this.

Figure 13 shows the total multi-group cross section up to 5 MeV (bining of 100 keV). At energies below 2 MeV, the JEFF-40T1 total cross section is slightly different from the others. Above 2 MeV, it is the TENDL-21 cross section that differs. The balance between elastic and inelastic scattering is therefore the important point above 2 MeV.
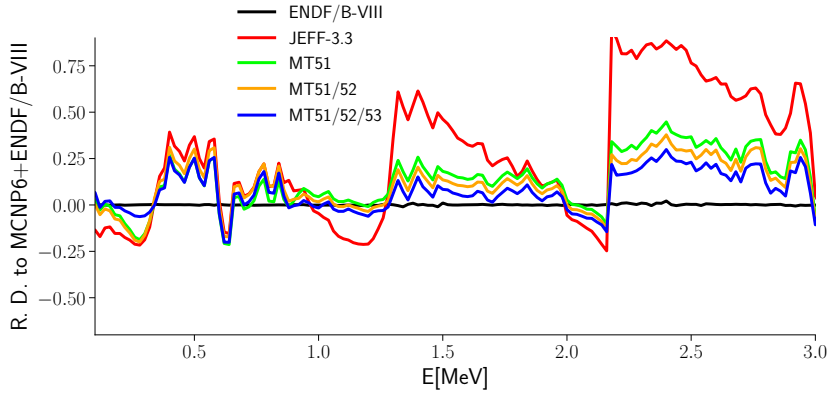
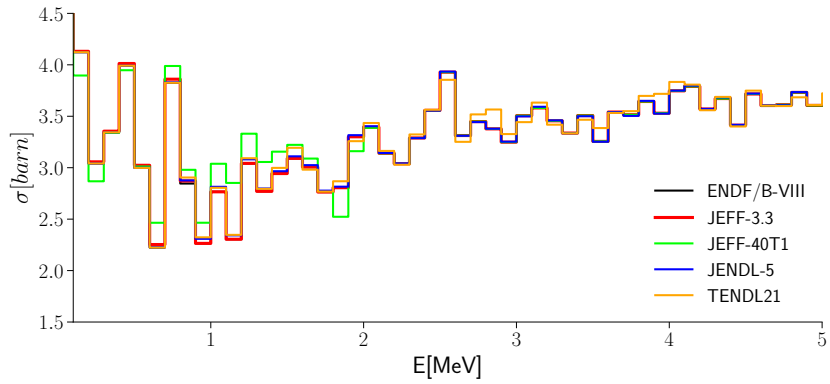Figure 12: Fe56 Slowing down 3 MeV. Impact of inelastic scattering

Figure 13: Fe56 Multigroup total cross-section (bining of 100keV)

4 ASPIS benchmark

The goal of this experiment is to test nuclear data and calculation methods on a configuration close to those of light water reactors. This experimental device is installed on the NESTOR reactor at Winfrith. A fission source is driven by thermal neutrons leaking from the outer graphite reflector of NESTOR. This benchmark was realised to study the propagation of neutrons in an iron bulk. The main nucleus in the composition structure is 56Fe whose evaluation is done using linear-linear interpolation in energy-angle distributions (in particular for continuous inelastic scattering with a threshold at 4.5 MeV). Three high energy dosimetric responses are measured at different depths of penetration in the iron bulk (from 5.5 to 114 cm) :

- 103Rh(n,n') reaction with an energy threshold of 40 keV

- 115In(n,n') reaction with an energy threshold of 339 keV

- 32S(n,p)32P reaction with an energy threshold of 1.0 MeV

The cumulative systematic and statistic errors for the dosimeters are respectively : 14% for 103Rh, 7:5% for 115In and 10% for 32S.

4.1   TRIPOLI-4 calculations using various libraries

Figure 14 shows the neutron propagation results in the iron bulk as a C/E ratio for the three dosimeters mentioned. The calculations are performed with TRIPOLI-4 and the previous libraries.
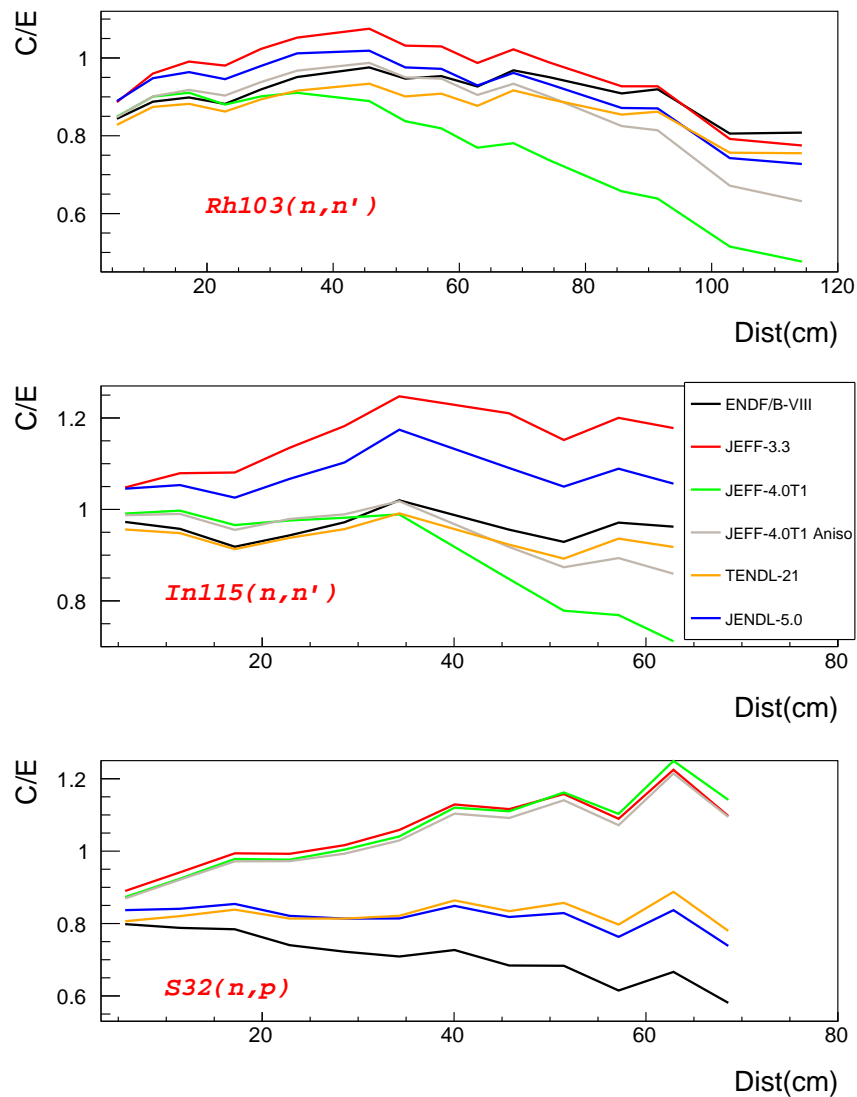

Figure 14: Aspis benchmark. C/E for three dosimeters.

In the following figures (15 and 16), the ENDF/B-VIII library is used for all nuclei except Fe56. The evaluations of the different libraries are then used. The impact of this nucleus for this benchmark can be seen by comparison with Figure 14. The differences are very large and are related to both the differences in the elastic scattering anisotropies and the discrete inelastic scattering cross sections (Figure 16).
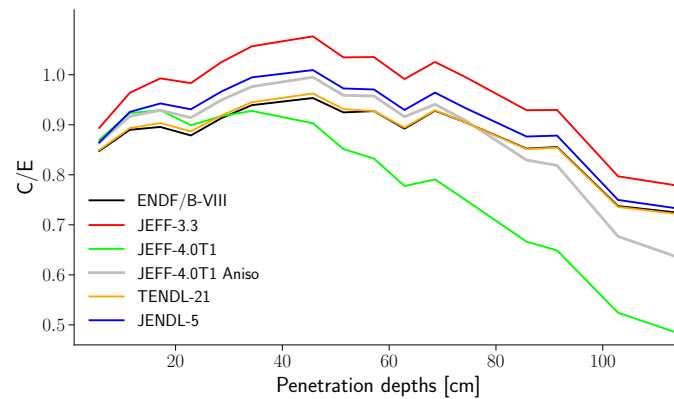

Figure 15: Aspis Rh103 C/E comparison using complete ENDF/B-VIII library except for Fe56 from different libraries
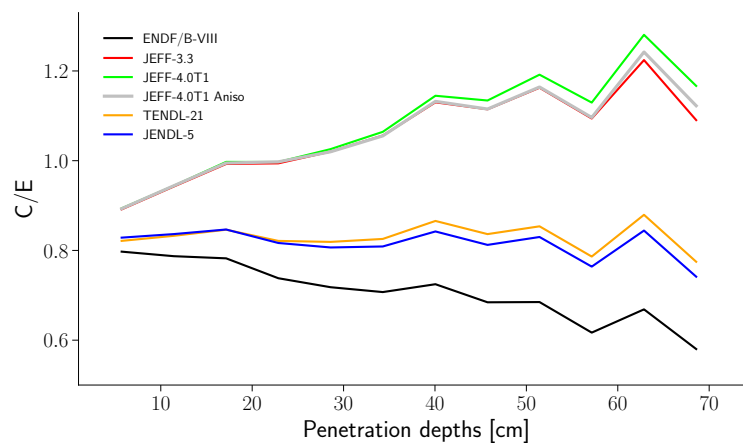

Figure 16: Aspis S32 C/E comparison using complete ENDF/B-VIII library except for Fe56 from different libraries

Figure 17 and Figure 18 show the results obtained with several combinations of Fe56 evaluations from ENDF/B-VIII and JEFF-3.3 :

- Fe56 from ENDF/B-VIII (black)

- Fe56 from JEFF-3.3 (red)

- Fe56 from JEFF-3.3 with elastic scattering anisotropy (MF4/MT2) from ENDF/B-VIII (green)

- Fe56 from JEFF-3.3 with MF3/MT51 from ENDF/B-VIII (grey)

- Fe56 from JEFF-3.3 with MF3/MT51-MT52-MT53 from ENDF/B-VIII (orange)

- Fe56 from JEFF-3.3 with MF3/MT51-MT52-MT53 and MF4/MT2 from ENDF/B-VIII (blue)

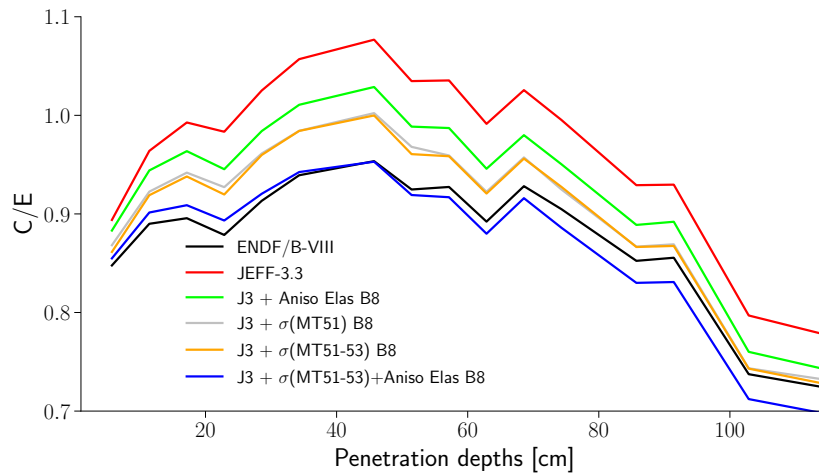All others evaluations are from ENDF/B-VIII

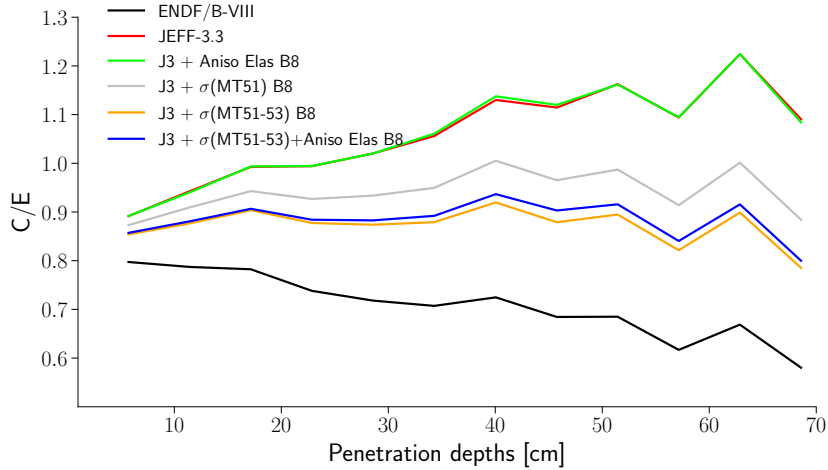Figure 17: Aspis Rh103 C/E analysis. Differences between JEFF-3.3 and ENDF/B-VIII

Figure 18: Aspis S32 C/E analysis. Differences between JEFF-3.3 and ENDF/B-VIII

5 Criticality benchmarks

Tests on HMF-014 and PMF-028 criticality benchmarks using Fe56 evaluation files from the different libraries. Table 1 presents results obtained with all nuclei from ENDF/B-VIII and the following Fe56 evaluation files :

- Fe56 from ENDF/B-VIII : Fe56_B8

- Fe56 from JEFF-3.3 : Fe56_J3

- Fe56 from JEFF-3.3 with elastic scattering anisotropy (MF4/MT2) from ENDF/B-VIII : Fe56_J3_A2B8

- Fe56 from JEFF-3.3 with MF3/MT51 from ENDF/B-VIII : FE56_J3_X51B8

- Fe56 from JEFF-3.3 with MF3/MT51-MT52-MT53 from ENDF/B-VIII : Fe56_J3_X53B8

- Fe56 from JEFF-3.3 with MF3/MT51-MT52-MT53 and MF4/MT2 from ENDF/B-VIII : Fe56_J3_X53A2B8

Several comments can be made with these results :

- The impact of the difference in anisotropy on the elastic scattering between the two evaluations is of the same order of magnitude as the difference between the two calculations using the two full Fe56 evaluations (ENDF/B-VIII and JEFF-3.3)

- Differences in inelastic scattering cross sections to the first excited state (MF3/MT51) have an impact of the order of 100 pcm on these benchmarks

Table 1: TRIPOLI-4 k_{eff} calculated using various Fe56 evaluation file

Eval/Bench.	HMF-014	PMF-028
Experimental	0.99890 (170)	1.00000 (220)
Fe56_B8	1.00084 (3)	1.00425 (3)
Fe56_J3	0.99625 (3)	0.99886 (3)
FE56_J3_A2B8	1.00031 (3)	1.00414 (3)
Fe56_J3_X51B8	0.99780 (3)	1.00066 (3)
Fe56_J3_X53B8	0.99800 (3)	1.00087 (3)
Fe56_J3_X53A2B8	1.00202 (3)	1.00606 (3)

- The differences in the inelastic scattering towards the higher excited states are much smaller, of the order of 20 pcm (the calculations are statistically converged at 3 pcm)

- The combination of changes in cross-sections (MF3/MT51-53) and elastic scattering anisotropy (MF4/MT2) over-corrects the differences between JEFF-3.3 and ENDF/B-VIII. This shows that this method of modifying block data in the evaluations is not very physical. There are compensations to be taken into account.

- If the inclusion of non-physical backgrounds cross section for capture and elastic 19 in the resolved resonance range (i.e. ENDF/B-VIII.0) allow to quickly adjust criticality benchmarks C/E 20 this also does induce un-physical flux and reaction rates profile in shielding, slowing down benchmarks
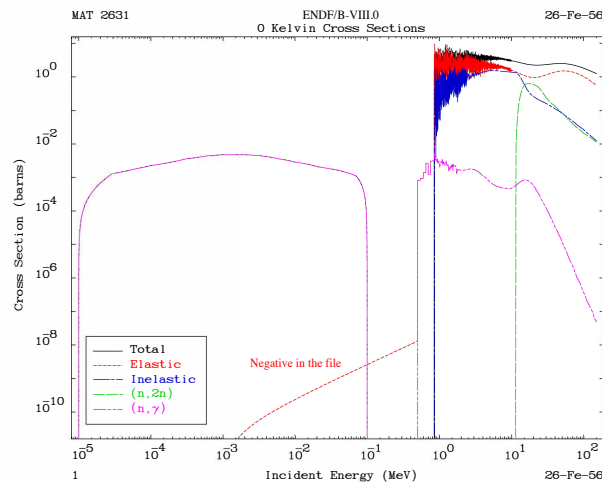

Figure 19: ENDF-6 forms of ENDF/B-VIII.0 backgrounds cross section in the RRR
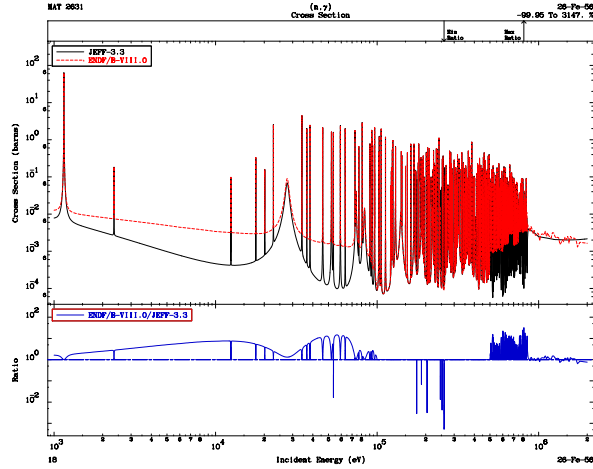
13

Figure 20: JEFF-3.3 versus ENDF/B-VIII.0 capture

6 Conclusions

These studies show the impact of differences in elastic scattering anisotropy and inelastic scattering cross-sections for Fe56 on simple slow-down configuration in mono-atomic medium and in study configurations used in criticality and shielding. It clearly highlight that more consideration need to taken by evaluator in shaping cross section profiles aiming at better integral C/E. Anisotropy, leakage, slowing-down aspects also needs to be properly factor in, interpreted if one want to deliver sound evaluations for multi-applications. The high energy, above resonance parts of a structural material evaluation need be properly evaluated, assembled and interpreted in shielding benchmarks prior thinking adjustment or tweak in its resonance range.

References

[1] D. Brown et al. *ENDF/B-VIII. 0: the 8th major release of the nuclear reaction data library with CIELO-project cross sections, new standards and thermal scattering data*, Nuclear Data Sheets, 2018, **148**, p. 1-142.

[2] A. Plompen et al. *The joint evaluated fission and fusion nuclear data library, JEFF-3.3.*, The European Physical Journal A, 2020, **56.7**, 1-108.

[3] https://www.oecd-nea.org/dbdata/jeff/jeff40/t1/

[4] Iwamoto & al. *Status of JENDL*, EPJ Web of conferences, 2020, **239**,09002

[5] A. Koning et al. *TENDL: complete nuclear data library for innovative nuclear science and technology.* Nuclear Data Sheets, 2019, **155**, 1-55.

[6] V. Raffuzzi1 et al *An iron evaluation story: from TALYS model parameters to validation on the ASPIS benchmark with the Monte Carlo code TRIPOLI-4.* ANS PHYSOR 2022 `doi.org/10.13182/PHYSOR22-37310`, 2022.

[7] E. Brun et al., *Tripoli-4, CEA, EDF and AREVA reference Monte Carlo code*, Annals of Nuclear Energy, 2015, **82**, 151-160.

[8] T. Goorley et al. *Features of MCNP6*. SNA+ MC 2013-Joint International Conference on Supercomputing in Nuclear Applications+ Monte Carlo. EDP Sciences, 2014. 06011.